GIS STATUS REPORT

M.Tashiro, Y.Fukazawa, E.Idesawa, Y.Ishisaki, H.Kubo,
K.Makishima (Univ. of Tokyo), Y.Ueda (ISAS) and the GIS team

May 9, 1995

1 Gain History

Figure 1 shows the long-term gain history of the two GIS detectors since the launch till April 1995. The plots refer to peak channels (PH) of the in-flight ^{55}Fe calibration isotope, corrected for the temperature effects. The new data points seem to lie on the extrapolation from the previously reported trend (Ishida et al. 1994). This slow gain decrease is possibly due to a slow decrease in the ultraviolet transmission of quartz windows of the gas cell and the phototube, through e.g. gradual developments of cosmic-ray induced crystalline defects. As of April 1995, the GIS performance has otherwise remained essentially constant since the launch. In particular, we have noticed no change in the rise-time characteristics or the energy resolution of either GIS sensor.

2 The New 'gain map' Released in February 1995

2.1 The gain map

The raw pulse-height (PH) of each GIS event is converted to energy (PI) in reference to conversion factors specified by a 'teldef file'. Since the intrinsic GIS gain is not only temperature sensitive but also position dependent due to non-uniformity in the phototube gain, this conversion process involves a look-up table called 'gain map' (Ishida et al. 1994). The gain map summarizes relative gains of each sensor (S2 or S3) as a function of the position of event incidence. The first version of gain maps were generated based on the extensive pre-launch calibration. In order to compensate for possible gain perturbation (especially in the phototube dynodes) at the launch, we then updated the gain maps through in-orbit measurements

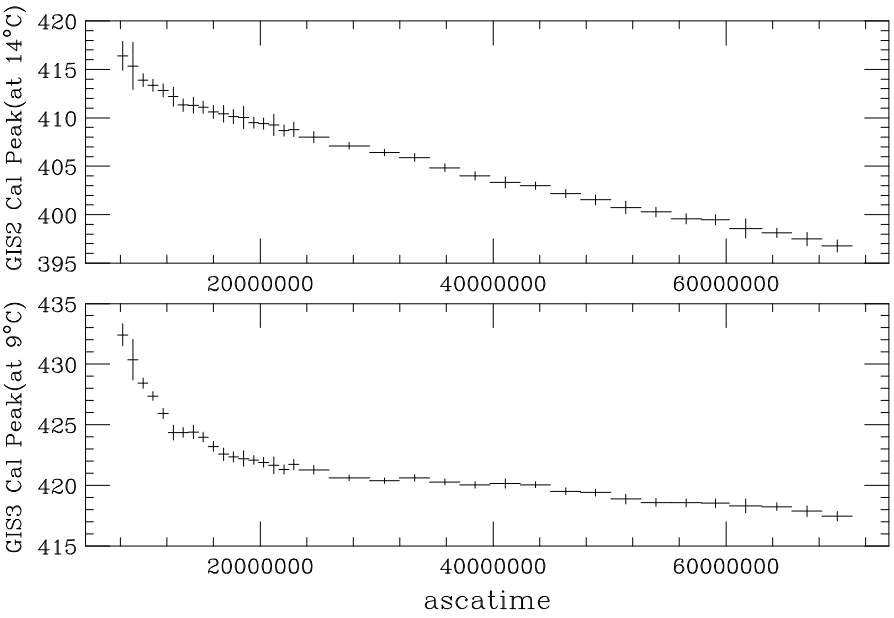

Figure 1: The long-term gain history of the two GIS detectors since the launch till April 1995 (see text).

of iron-K lines from clusters of galaxies and supernava remnants. However the uncertainty remained relatively large near the outer rim of the detector (Ishida et al.1994).

2.2 Updated gain maps

In order to further calibrate the GIS gain maps, we have accumulated 2000 ks of data both from the solar irradiated earth ('day earth') and the 'night earth'. Though scientifically useless, these data provide excellent opportunity of calibrating the gain maps. In fact the day earth data exhibit strong K-emission lines from ionized magnesium, silicon and sulphur of solar origin, as well as neutral argon-K line via atmospheric fluorescence (Kubo et al. 1994). Whereas in the night and day earth data, we see copper-K lines at 8.04 keV which are emited from support ribs of the detector window through activation by charged particles (Kubo et al. 1994).

These atomic lines are advantageous because they rather uniformly spread over the entire detector fields, allowing us to better calibrate relative gains towards the outer edges of the field of view. Furthermore, these earth data can be routinely accumulated for progressively longer times even in the guest observation phase.

Based on these data, we have updated the gain maps for both S2 and S3. Figure 2 shows maps of the ratios of the new gain map to the old one. They indicate that the tune-up has been most significant (up to 6 % relatively) for the outermost regions of S3.

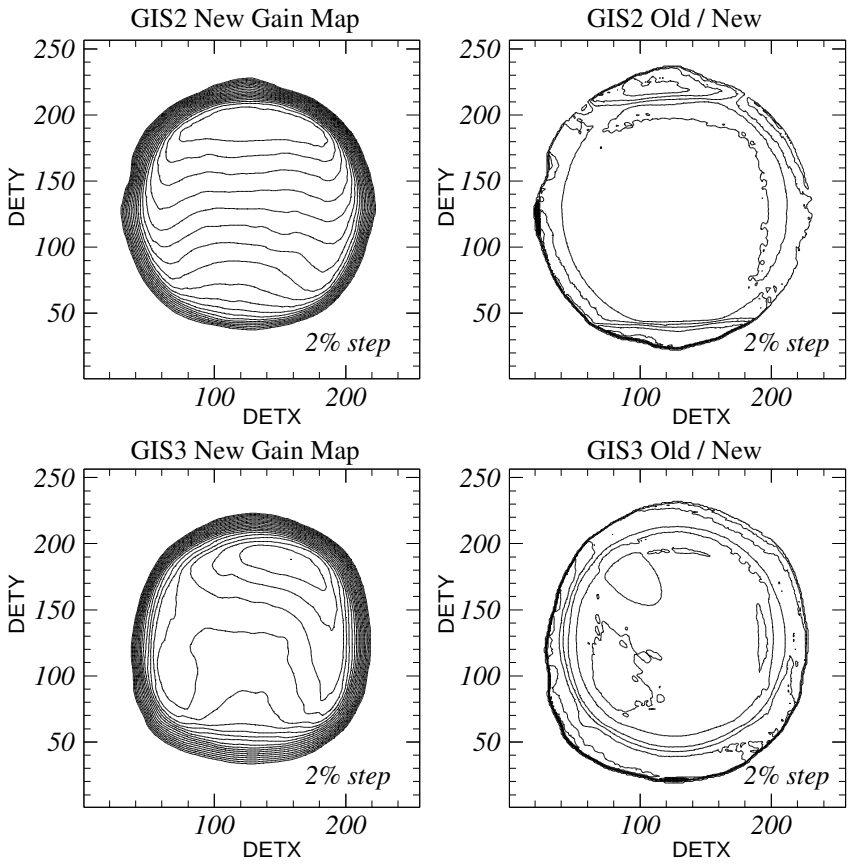

Figure 2: Maps of the ratios of the new gain map to the old one.

2.3 Release of new teldef files in February 1995

On February 21, 1995, we have released the the new 'teldef files' which are based on the new gain maps as described above. These files are supplied to guest observers as

`/caldb/data/asca/gis/bcf/gis2_ano_on_flf_180295.fits`...(for S2)
and
`/caldb/data/asca/gis/bcf/gis3_ano_on_flf_180295.fits`...(for S3).

In the previous gain map, the reliablity within ± 2 % and $+6/-2$ % were guaranteed within and outside 15 arcmin from the center, respectively. Now in the new version of gain maps, the reliability is improved to ± 1 %, ± 2 % and ± 4 % for the region within 15 arcmin, $15-20$ arcmin and $20-50$ mm, respectively, for both detectors. This is illustrated in Fig.3, namely plots of the copper-K line energy in the inner and

outer regions, obtained with the old and new gain maps.

When using the updated 'teldef' file together with the rmf files supplied so far, the center energy of K-alpha line from the calibration isotope will turn out to be at 5.94 keV and 5.97 keV for S2 and S3, respectively. This may give guest obervers a useful confirmation of proper reduction of the GIS data. (The isotope emits 5.8942 keV Mn-K alpha line for reference.)

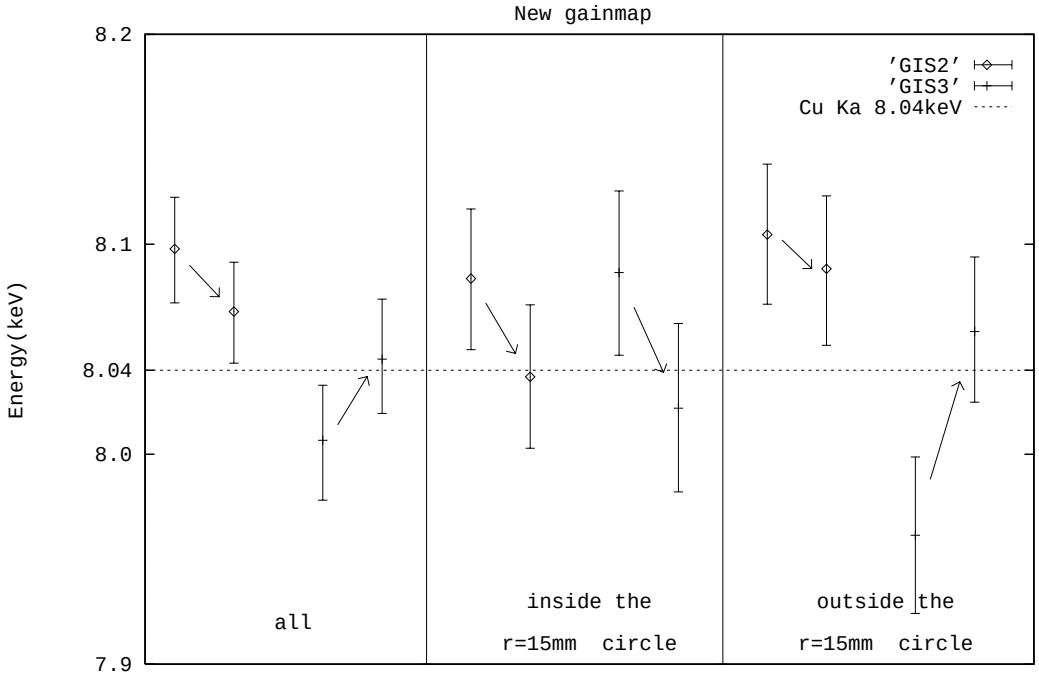

Figure 3: Plots of the copper-K line energy in the inner and outer regions, obtained with the old and new gain maps.

3 Relase of new 'rmf' file in March 1995

3.1 Remaining problems in rmf

Based primarily on the ground calibration, the GIS energy redistribution matrix (rmf) has been updated in orbit referring to the Crab Nebula data, so that its spectrum can be fitted with a power-law of photon index ~ 2.1 and photoelectric absorption with $N_{\rm H} \sim 3 \times 10^{21}$. The previous version of the rmf successfully reproduced the Crab spectrum within 4 %, in the 0.7 – 10 keV energy range where the GIS is most sensitive. However below ~ 1 keV, the model covolved through rmf tend to underpredict the flux (Fig.2 of Ishida et al. 1994).

Since the GIS window (10 μm thick beryllium foil) becomes quite opaque to X-rays below ~ 0.7 keV, the GIS events appearing below this energy are thought primarily to come through 'spill-over' of higher energy events. That is, the pulse-height response of the GIS (and of gas scintillation proportional counters in general) for monochromatic X-rays is known to deviate from a single Gaussian, exhibiting a tail toward lower energies (Inoue et al. 1978; Kohmura et al. 1993). This is caused by the fractional capture of primary electrons by the X-ray entrance window. This effect can be modeled in terms of a single parameter, $\kappa = \mu D/\omega$, where μ, D and ω stand for X-ray absorption coefficient of Xenon gas, diffusion coefficient of primary electrons, and electron drift velocity along the electric field, respectively (Inoue et al. 1978). The soft-energy tail is insignificant when $\kappa = 0$, and becomes prominent as κ approaches 1.

To improve the rmf file, we reviewed the entire pre-launch calibration data, including those obtained in the UV SOR experiment (Kohmura et al. 1993). We also utilized in-orbit data of sources with various column densities; GRS 1915+105 ($N_{\rm H} = 4 \times 10^{22}$ cm^{-2}), EXO 2030 ($N_{\rm H} = 2 \times 10^{22}$ cm^{-2}), The Crab Nebula ($N_{\rm H} = 3 \times 10^{21}$ cm^{-2}), and 3C273 ($N_{\rm H} = 3 \times 10^{20}$ cm^{-2}). Referring to these data sets, we updated the value of k, improved the calculation code, and re-evaluated energy resolution toward very low pulse heights. We also performed fine tunings of the lower-most end of the soft tail for photons with energies above 2.5 keV.

Through these improvements we have generated updated rmf files, which have been released in March 1995 as

`/caldb/data/asca/gis/cpf/95mar06/gis2v4_0.rmf`...(S2)
and
`/caldb/data/asca/gis/cpf/95mar06/gis3v4_0.rmf`...(S3).

Figure 4 shows representative GIS spectra fitted with the old and new rmf files. Improvements in the fit below 1 keV is evident. However we have to mention that a broad line like feature still remains in the fit residual around 5 keV, with deviation of about 4 % at peak, as is seen in the Crab spectra in Fig.4. We understand that the artifact is caused by discontinuity in the response function, which will be reduced in cooperation with the XRT team in the next version of response function.

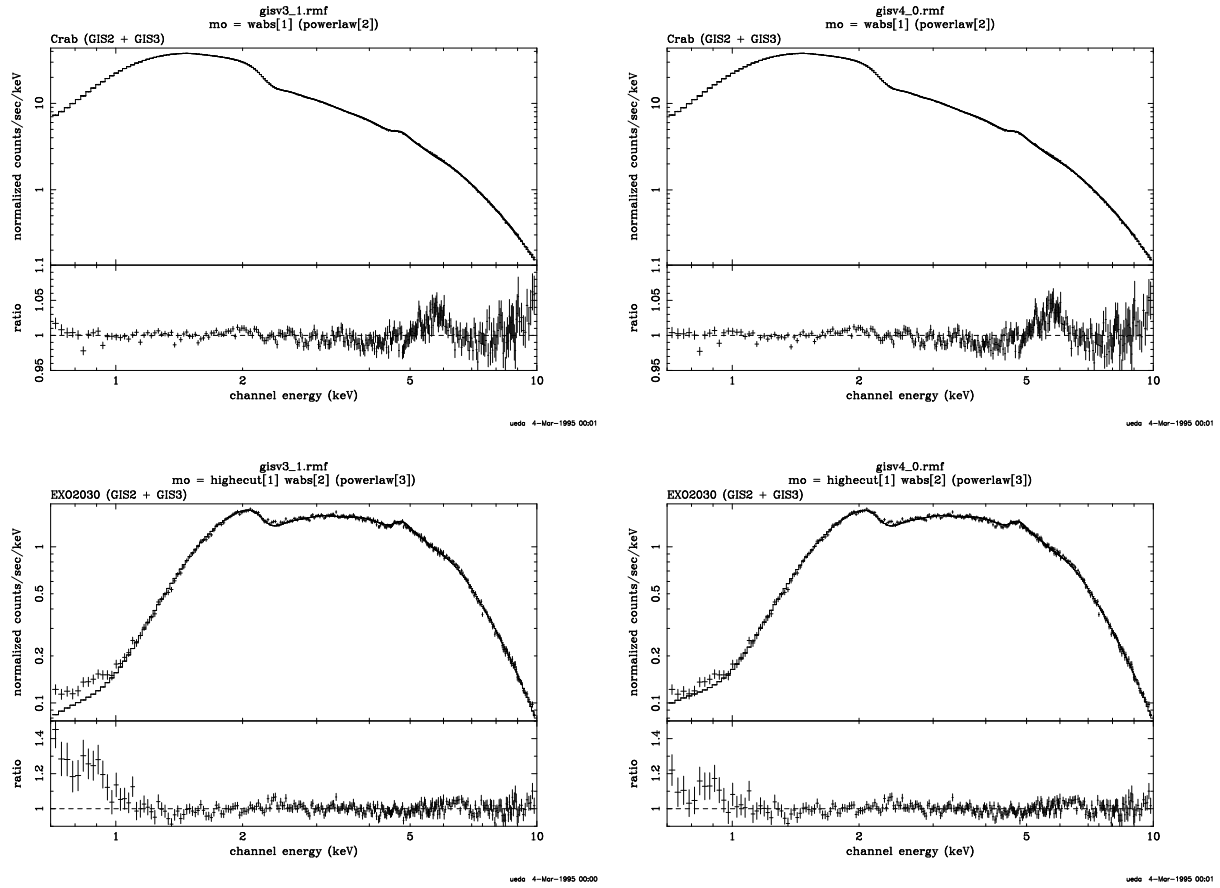

Figure 4: Representative GIS spectra fitted with the old (gisv3_1.rmf) and the new (gisv4_1.rmf) rmf files. The spectra are obtained from Crab nebula are displayed in upper pannels, and left and right ones are fitted using the old and new rmfs respectively. Spectra from EXO 2030 are displayed in lower pannels in the same way for Crab specttra. All spectra are obtained from both two GIS sensors.

References

Inoue, H. et al. 1978, Nucl. Instr. and Meth. vol. 157, p.295.

Ishida, M. et al. 1994, ASCA News No.2, p.20.

Kohmura, Y. et al. 1993, SPIE vol. 2006, p.78.

Kubo, H. et al. 1994, ASCA News No.2, p.14.